Analysis and trajectory planning for anti-swing on a one-stage cart pendulum

Dan Wang[1,*], *Xinlu* Yu[2,3] and *Jiangzhao* Yang[3]

[1]School of Mechanical and Electrical Engineering, Guangdong University of Science and Technology, Dongguan, China
[2]Laboratory of Intelligent Manufacturing and Precision Machining, Tsinghua Shenzhen International Graduated School, Tsinghua University, Shenzhen, China
[3]Department of Research and Development, Googol Paradox (Dongguan) Intelligent Technology Co., Ltd., Dongguan, China

Abstract. In order to achieve smooth and anti-swing positioning process, a smooth trajectory planning scheme, which is mainly the linear combination of trigonometric functions, is proposed for a one-stage cart pendulum. Based on the internal dynamics of the cart pendulum system, the planning trajectory of the cart is derived from the anticipated swing angle of the pendulum bar, which satisfies the initial and terminal state constraints. Experiments are conducted to demonstrate the performance of anti-swing with the introduced planned trajectory.

1 Introduction

Pendulum on cart is a typical under-actuated system in physical applications. Within this system, the cart translation causes the pendulum to swing back and forth, which not only reduces the efficiency of the transferring but also leads to potential risks of hitting. The main control objectives of positioning in such system can be summarized in moving the cart to arrive at the desired position within a short time and suppressing the pendulum swing within a given domain for safety reasons.

Numerous researchers have studied the anti-swing control problem and proposed different control strategies for the under-actuated cranes described in [1]. The transition task is treated as a two-point boundary value problem in [2] to deal with the anti-swing and position control. In [3], a kinematic coupling-based off-line trajectory planning method is proposed to achieve smooth trolley transportation and small payload swing. Optimal sliding mode control method is applied in [4], while inverse transfer function method is taken into account in [5]. A control approach based on a model predictive control and a particle swarm optimizer is proposed for limiting the transient and residual swing in [6]. Closed-loop signal shaping is utilized in [7] by placing the Smith predictor inside the feedback loop to improve manual control of a 3D crane. Trapezoidal acceleration spline curve

* Corresponding author: wangdanhbyc@hotmail.com

programming and backstepping control strategy are applied for anti-swing and positioning in [8] and [9], respectively. In [10], a controller is designed for the under-actuated system with the knowledge of differential flatness. Meanwhile, optimal preview control is applied to complete the rapid positioning and swing angle suppression when utilizing the future information in [11].

Generally, trajectory planning and advanced control algorithm design are two available techniques to achieve the smooth and anti-swing transferring for the under-actuated systems. However, trajectories in the previous works were obtained only from the system kinematics, dynamics of the overall system was out of attendance when generating the trajectories. In this paper, focusing on the aspect of trajectory planning, a smooth trajectory planning scheme is proposed for a one-stage cart pendulum based on the internal dynamics of the physical system. In terms of the anticipated swing angle of the pendulum bar, the planning trajectory of the cart is derived from mostly the linear combination of sine and cosine functions, with specified initial and terminal state constraints. Simulation and experiments have been conducted to demonstrate the anti-swing performance of the introduced planned trajectory on a physical platform.

2 Model of the one-stage cart pendulum

As depicted in figure 1, the one-stage cart pendulum consists of a straight-line rail, a cart, a pendulum bar, and a driving unit, which drives the cart via a toothed belt by a synchronous motor. A pre-tuned velocity-loop controller of the synchronous motor is configured, such that an ideal control of the cart's speed can be presumed. In figure 1, XOY is the reference frame of the system, while the rest of notions are described in table 1. It is reasonable to assume that the mass of the pendulum bar is uniformly distributed.

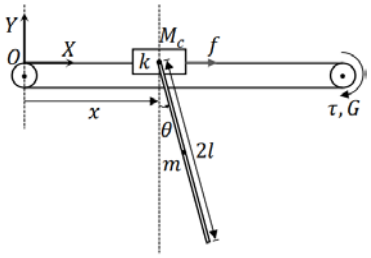

Fig. 1. Schematic diagram of the one-stage cart pendulum.

According to the Lagrange's equations, the equations of motion for the one-stage cart pendulum could be derived as

$$(M_c + m)\ddot{x} + ml\dot{\theta}\cos\theta - ml\dot{\theta}^2 \sin\theta = f \tag{1}$$

$$ml\ddot{x}\cos\theta + \frac{4}{3}ml^2\ddot{\theta} + mgl\sin\theta = -k\dot{\theta} \tag{2}$$

Equation (1) represents the actuated part of the system, while equation (2) denotes the underactuated part, which describes the coupling dynamics of the cart displacement and pendulum swing angle. As the dynamics of the cart is fully controlled by the synchronous motor, the acceleration of the cart could then be chosen as a substitute for the new control

input u , i.e., equation (1) is replaced by $\ddot{x} = u$. Furthermore, approximations of $\cos\theta$=1 and $\sin\theta$=θ hold for a small swing angle. Thereby, the dynamics of the one-stage cart pendulum becomes

Table 1. Notations in the schematic diagram.

	Representation	Value
M_c	Mass of cart	/
x	Cart placement	/
G	Gear ratio	/
τ	Motor torque	/
$f = G\tau$	Control force	/
θ	Pendulum angle	/
m	Mass of pendulum	0.105(kg)
l	Half-length of pendulum	0.25(m)
k	Friction coefficient of joint	-0.0096
g	Acceleration of gravity	9.81(m/s^2)

$$\ddot{x} = u \tag{3}$$

$$\ddot{x} + k_1\ddot{\theta} + k_2\dot{\theta} + g\theta = 0 \tag{4}$$

Where $k_1 = \frac{4}{3}l$ and $k_2 = \frac{k}{ml}$. Equation (4) is defined as the internal dynamics of the cart pendulum.

3 Trajectory planning

3.1 Initial and terminal states in positioning

Taking the system of figure 1 into considered, a positioning movement represents the cart, taking with the pendulum bar, moves from one position to another setpoint position in a finite translation time. Once the desired position of the cart was achieved, the swing amplitude of the pendulum bar must be suppressed within an acceptable domain. That is, the pendulum bar is required to be anti-swing especially at the end of the cart motion.

Table 2 gives the initial states and terminal states for the one-stage cart pendulum when performing point-to-point cart translation in a finite moving time from x_0 to x_T in a finite moving time T_m . The top eight states are required for the smooth trajectory, while the last four states are required to meet the consistency of the control effort in the physical system.

Table 2. Initial states and terminal states in positioning.

	Initial state	Terminal state
Cart position	$x(0) = x_0 = 0$	$x(T_m) = x_T$
Pendulum angle	$\theta(0)=0$	$\theta(T_m) = 0$
Cart velocity	$\dot{x}(0)=0$	$\dot{x}(T_m) = 0$
Pendulum velocity	$\dot{\theta}(0) = 0$	$\dot{\theta}(T_m) = 0$
Cart acceleration	$\ddot{x}(0) = 0$	$\ddot{x}(T_m) = 0$
Pendulum acceleration	$\ddot{\theta}(0) = 0$	$\ddot{\theta}(T_m) = 0$

3.2 Trajectory generation

Suppose x^* and θ^* were the solution for the internal dynamics, i.e., equation (4), there exists

$$\dddot{x}^* + k_1\ddot{\theta}^* + k_2\dot{\theta}^* + g\theta^* = 0 \tag{5}$$

Then, the input u^* that satisfied $u^* = \ddot{x}^*$ would guarantee the desired trajectories of the cart and the pendulum. According to table 2, the desired trajectory of the pendulum, θ_d^*, can be constructed in the following form

$$\theta_d^*(t) = -2p\sin\omega_2 t + p\sin\omega_4 t \tag{6}$$

where p is the free parameter depending on the initial and terminal constraints and $\omega_i = i\pi / T_m$ with $i = 2,4$. Taking the first and second derivatives of (6), the desired velocity and acceleration of the pendulum are

$$\dot{\theta}_d^*(t) = -2p\omega_2\cos\omega_2 t + p\omega_4\cos\omega_4 t \tag{7}$$

$$\ddot{\theta}_d^*(t) = 2p\omega_2^2\sin\omega_2 t - p\omega_4^2\sin\omega_4 t \tag{8}$$

Obviously, equation (7) and equation (8) automatically satisfy the corresponding constraints in table 2, due to the periodical properties of sinusoidal functions. Substituting equation (6) to equation (8) into equation (5), the desired dynamic of the cart comes from

$$\ddot{x}_d^*(t) = -\left(k_1\ddot{\theta}_d^*(t) + k_2\dot{\theta}_d^*(t) + g\theta_d^*(t)\right) \tag{9}$$

Clearly, $\ddot{x}_d^*(0) = \ddot{x}_d^*(T_m) = 0$ was satisfied. With the first and second integral of equation (9), the desired cart velocity and position would be derived from

$$\dot{x}_d^*(t) = -\left(k_1\dot{\theta}_d^*(t) + k_2\theta_d^*(t) + g\bar{\theta}_d^*(t)\right) \tag{10}$$

$$\ddot{x}_d^*(t) = -\left(k_1\theta_d^*(t) + k_2\bar{\theta}_d^*(t) + g\tilde{\theta}_d^*(t)\right) \tag{11}$$

With

$$\bar{\theta}_d^*(t) = \int_0^t \theta_d^*(\tau)\,\mathrm{d}\tau = 2\frac{p}{\omega_2}\cos\omega_2 t - \frac{p}{\omega_4}\cos\omega_4 t - 3\frac{p}{\omega_4} \tag{12}$$

$$\tilde{\theta}_d^*(t) = \int_0^t \bar{\theta}_d^*(\tau)\,\mathrm{d}\tau = 2\frac{p}{\omega_2^2}\sin\omega_2 t - \frac{p}{\omega_4^2}\sin\omega_4 t - 3\frac{p}{\omega_4}t \tag{13}$$

Moreover, for a desired terminal cart position, the free parameter would be obtained from

$$p = \frac{4\pi}{3g}\frac{x_T}{T_m^2} \tag{14}$$

On the other hand, once p was determined, the maximal magnitude of the desired swing angle of the pendulum in equation (6) could be generated from

$$\max_{t\in[0,T_m]}\left|\theta_d^*(t)\right| = \frac{3\sqrt{3}}{2}p = \frac{2\sqrt{3}\pi}{g}\frac{x_T}{T_m^2} \tag{15}$$

4 Simulation and experiments

4.1 Simulation

An instance of the desired trajectories with $x_T = 0.5(\mathrm{m})$ and $T_m = 2(\mathrm{s})$ was depicted in figure 2. Clearly in figure 2, the initial and terminal states meet the requirements in table 2. Figure 3 shows the corresponding discrete samples of the cart pendulum during the setpoint transition, where the pendulum angle changes smoothly.

4.2 Experiment

Experiments were performed on the one-stage cart pendulum, named GLIP2001 series, manufactured by Googol Paradox Technology to verify the anti-swing performance of the proposed trajectory planning approach. The experiment platform has a cart stroke of 0.6 meter, which is driven by a servo motor via a toothed belt. The servo motor, is operated in velocity-loop mode with an encoder adopting the resolution of 10000 pulses per revolution. Cart placement is measured through the encoder of the servomotor indirectly. That is, one pulse represents 0.46/37500.0 meter. Swing angle of the pendulum bar is obtained by an independent encoder with the resolution of 10000 pulses per revolution. Commands and

feedback signals are manipulated by the PC-based motion controller, GT-400-SV, provided by Googol Technology. Real-time controls, feedforward and feedback control schemes, are handled by means of the real-time toolbox in SIMULINK environment.

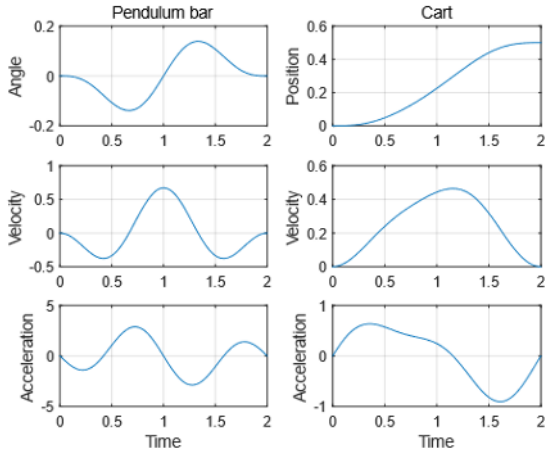

Fig. 2. Instance of desired trajectories.

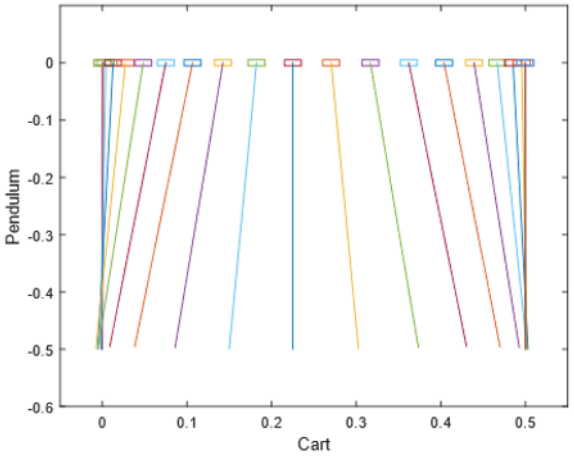

Fig. 3. Transition from the initial state to the terminal state.

To evaluate the characteristics of the proposed trajectory, two sets of experiments were conducted on the experiment platform. The first set of experiments was designed with different terminal planning time to the same target position. Experiment results are show in figure 4, where the target cart position x_T is 0.5 meter and the terminal planning time T_m is 2, 3 and 4 seconds respectively. Numerical results are concluded in table 3, where the theoretical maximum values are obtained from equation (15) when substituting $x_T = 0.5$ and $T_m = 2$, 3 and 4 respectively. Clearly, the shorter the terminal planning time was adopted, the larger swing angle would be produced. Moreover, the pendulum keeps steady after the cart arrived the desired terminal position. Purpose of anti-swing is achieved via the proposed trajectory planning scheme.

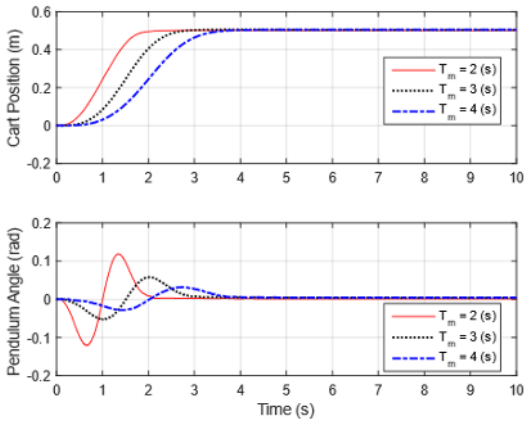

Fig. 4. Trajectory with different terminal time to same target position.

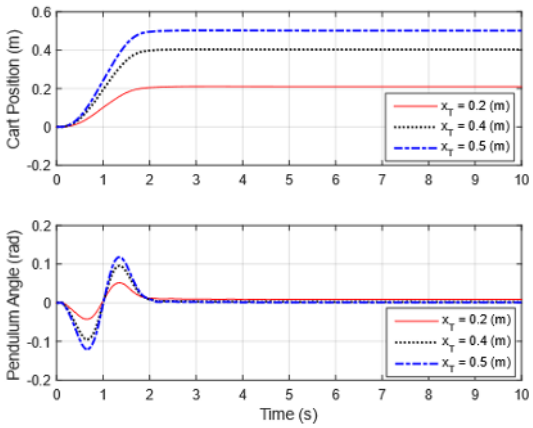

Fig. 5. Trajectory with different target position at same terminal time.

In the second set of experiments, terminal planning time was fixed as 2 seconds, while the target cart position was set from 0.2 meter to 0.5 meter. Experiment and numerical results are given in figure 5 and table 4, respectively. It could be found that, for a specific terminal planning time, the longer moving target position generates a larger pendulum swing angle.

Table 3. Results in different planning time.

Planning time (s)	Max pendulum angle (rad)	
	Theoretical	Actual
2	0.1387	0.1206
3	0.0616	0.0578
4	0.0347	0.0320

Table 4. Results in different target position.

Target position (m)	Max pendulum angle (rad)	
	Theoretical	Actual
0.2	0.0555	0.0522
0.4	0.1109	0.0955
0.5	0.1387	0.1206

5 Conclusion

In this paper, a smooth trajectory planning approach, which is mainly the linear combination of sine and cosine functions, is proposed for the anti-swing setpoint transferring process of a one-stage cart pendulum. Based on the internal dynamics of the cart pendulum system, the planning trajectory of the cart is derived from the anticipated swing angle of the pendulum bar, which satisfies the initial and terminal state constraints. To illustrate the anti-swing performance of the introduced trajectory planning scheme, simulation and experiments are conducted and tested on a physical platform.

This work is supported by the 2020 Young Innovative Talents Project of Guangdong Ordinary Colleges and Universities (NO. 2020KQNCX104), the General Project of Social Science and Technology Development of Dongguan City (NO. 2020507154647) and the Higher Education Teaching Reform Project of Guangdong University of Science and Technology (NO. CQ2020095).

References

1. E. M. Abdel-Rahman, A. H. Nayfeh and Z. N. Masoud, “Dynamics and control of cranes: A review,” Journal of Vibration Control, vol. 9(7), pp. 863-908, 2003.
2. T. Glück, A. Eder and A. Kugi, “Swing-up control of a triple pendulum on a cart with experimental validation,” Automatica, vol. 49(3), pp. 801-808, 2013.
3. N. Sun, Y. Fang, Y. Zhang and B. Ma, “A novel kinematic coupling-based trajectory planning method for overhead cranes,” in IEEE/ASME Transactions on Mechatronics, vol. 17(1), pp. 166-173, 2012.
4. Z. Sun, X. Zhao, Z. Sun, F. Xiang and C. Mao, “Optimal sliding mode controller design based on dynamic differential evolutionary algorithm for under-actuated crane systems,” IEEE Access, vol. 6, pp. 67469-67476, 2018.
5. R. Voliansky et al., “Anti-swing control system for the one class of underactuated dynamic objects,” 2020 IEEE Problems of Automated Electrodrive. Theory and Practice (PAEP), 2020, pp. 1-4.
6. J. Smoczek and J. Szpytko, “Particle swarm optimization-based multivariable generalized predictive control for an overhead crane,” in IEEE/ASME Transactions on Mechatronics, vol. 22(1), pp. 258-268, 2017.
7. K. Yaovaja, W. Chatlatanagulchai and P. Yaemprasuan, “Anti-delay closed-loop input shaper to improve manual control of flexible system,” 2017 American Control Conference (ACC), 2017, pp. 4498-4503.

8. C. Liu, B. Sun and F. Li, “Acceleration planning based anti-swing and position control for double-pendulum cranes,” 29th Chinese Control and Decision Conference (CCDC 2017), 2017, pp. 5671-5675.
9. Y. Li, S. Zhou and H. Zhu, “A backstepping controller design for underactuated crane system,” 30th Chinese Control and Decision Conference (CCDC 2018), 2018, pp. 2895-2899.
10. Z. Zhang, Y. Wu and J. Huang, “Motion and anti-swing control of underactuated bridge cranes using differential flatness,” 35th Chinese Control Conference (CCC 2016), 2016, pp. 527-532.
11. R. Li, W. Tang and H. Gao, "Anti-swing design of an overhead crane based on optimal preview control," 40th Chinese Control Conference (CCC 2021), 2021, pp. 2532-2536.